Electronic properties investigation of human dihydrofolate reductase complexes with ligands

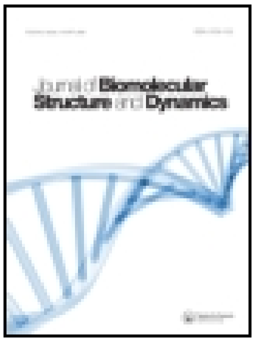

Journal of Biomolecular Structure and Dynamics

ISSN: (Print) (Online) Journal homepage: https://www.tandfonline.com/loi/tbsd20

Electronic properties investigation of human dihydrofolate reductase complexes with ligands

Vladislav Naumovich , Maria Grishina , Jurica Novak , Prateek Pathak , Vladimir Potemkin , Mohd Shahbaaz & Magda H. Abdellattif

JOURNAL OF BIOMOLECULAR STRUCTURE AND DYNAMICS
https://doi.org/10.1080/07391102.2020.1861985

Electronic properties investigation of human dihydrofolate reductase complexes with ligands

Vladislav Naumovich[a], Maria Grishina[a], Jurica Novak[a], Prateek Pathak[a], Vladimir Potemkin[a], Mohd Shahbaaz[a,b] and Magda H. Abdellattif[c]

[a]Laboratory of Computational Modeling of Drugs, Higher Medical and Biological School, South Ural State University, Chelyabinsk, Russia; [b]South African Medical Research Council Bioinformatics Unit, South African National Bioinformatics Institute, University of the Western Cape, Bellville, Cape Town, South Africa; [c]Department of Chemistry, College of Science, Deanship of Scientific Research, Taif University, Taif, Saudi Arabia

Communicated by Ramaswamy H. Sarma

ABSTRACT

Despite the fact that there are already drugs for cancer, they still show strong toxicity to the human organism. That is why it is necessary to establish the factors affecting activity in order to develop new, more effective drugs aimed at tumor cells, minimizing harm to healthy cells. The present research is based on electronic properties calculation of the complexes using AlteQ approach. In the focus of this study are complexes of human dihydrofolate reductase (hDHFR) with a series of known inhibitors bound in the active site. Further, a statistical analysis was performed to establish the relationships between a myriad electronic characteristics and IC_{50}. The change in total volume and the change of own electrons number of hydrogen atoms in their atomic basins are identified as the descriptors correlating the most with the hDHFR inhibition potency. Additionally, two lipophilic parts of protein (Thr56, Ser59, Ile60 and Ile7, Val8, Ala9) were found, which act as a key factor in decreasing bioactivity. The depth analysis of intermolecular interactions showed that the interactions between water molecules and ligand play a crucial role in hDHFR inhibition. Furthermore, the molecular dynamics simulations were used for deeper understanding of the structural inhibition, each for 50 ns time scale in explicit water conditions. Thus, the AlteQ approach made it possible to determine the factors influencing the activity and evaluate them not only qualitatively, but also quantitatively.

ARTICLE HISTORY
Received 25 September 2020
Accepted 5 December 2020

KEYWORDS
Electron density; quantum theory of atoms; AlteQ approach; DHFR activity; DHFR-ligand complexes

Introduction

Targeted therapy is one of the most interesting and important methodologies for the treatment of cancer due to its selectivity and specificity against the cancerous cell. The primary aim of targeted therapy is facilitating the drugs into certain genes or proteins for binding and alteration concerning physiological pathways. This change in physiological signaling pathways leads to the reduction of cancer growth with minimal effect on normal cells (Padma, 2015). Targeted therapy can be applied either individually or in the combination with other drugs. Additionally, this specific treatment methodology can be used as personalized medicines (Huber & Huber, 2019).

Dihydrofolate reductase (DHFR) is one of the key enzymes, having great role in intracellular metabolism. In mammals, DHFR actively participates in conversion of dietary folic acid to 7,8-dihydrofolate (FH2) and 5,6,7,8-tetrahydrofolate (FH4). This bio-process is regulated by a cofactor nicotinamide adenine dinucleotide phosphate (NADPH) (Cario et al., 2011; Schober et al., 2019). FH4 acts as an important cofactor for the enzymes that catalyze the transfer of one-carbon groups (e.g. methyl and formyl groups) from one organic compound to another. Enzyme-catalyzedtransfer reaction is necessary for the further synthesis of various amino acids and purines. The role of this signaling pathway can be understood by the example that thymidylate synthase (TS) is an FH4 mediated enzyme that catalyzes the conversion of deoxyuridine monophosphate (dUMP) to deoxythymidine monophosphate (dTMP). So, unavailability of FH4 can inhibit the catalysis of this process that encourages DNA degradation and cell death (Arooj et al., 2013; Etienne et al., 2004; Longley et al., 2003; Stivarou et al., 2015).

The available literature about DHFR explains that this enzyme is a convenient and effective chemotherapy target (Hawser et al., 2006). Various DHFR inhibitors are used as antitumor (Abdelaziz et al., 2019), antibacterial (Hawser et al., 2006), and antiprotozoal (Gangjee et al., 2008) agents. A large number of DHFR inhibitors such as methotrexate, trimethoprim, pyrimethamine, trimetrexate, and cycloguanil are used as drugs because of their ability to influence the catalysis of folic acid conversion (Hashkes et al., 2014; Masters et al., 2003; Nduati et al., 2008). So, the research towards DHFR receptor protein inhibition via 2,4-disubstituted pyrimidine moiety are promoted by various new

CONTACT Vladislav Naumovich naumovichvo@susu.ru; Maria Grishina grishinama@susu.ru Higher Medical and Biological School, Laboratory of Computational Modeling of Drugs, South Ural State University, Chelyabinsk 454080, Russia

Supplemental data for this article can be accessed online at https://doi.org/10.1080/07391102.2020.1861985.

drug discovery programs because of their clinical efficacy and minimal health risk.

Electron diffraction and X-ray crystallography techniques are widely utilized to observe the distribution of electron density in a molecule. The electron density is an important element for determining the geometry of molecules and their binding characteristics. The boundaries of quantum systems are determined by specific properties of electron density. These measurements help to assess the properties of atoms, inter atomic bonds, molecular structures, and mechanisms of structural changes. Therefore, theoretical calculations of electronic characteristics such as estimation of the surface electron density and volume characteristics of large molecular systems will be useful for the development of new DHFR inhibitors. The present research utilized a methodology based on the AlteQ approach, which shows the reactivity and helps in predicting molecular properties (V. Potemkin & Grishina, 2018b; V. A. Potemkin & Grishina, 2008; V. A. Potemkin et al., 2009; E. Salmina et al., 2013).

This paper presents the electron characteristics of complexes of the crystals of heteromolecular human dihydrofolate reductase (hDHFR) with various ligands obtained by X-ray diffraction (Cody et al., 1998, 2015; Gangjee et al., 1998, 2009; Klon et al., 2002; Lamb et al., 2013; Zhang et al., 2011). DHFR inhibitors enter into the cell through an active carrier transport and remain inside after binding to the protein. Thus, determining the three-dimensional structure of the target and its binding site is an important step in the study (Singh et al., 2018).

In addition, the half maximal inhibitory concentration (IC_{50}) were taken for theoretical consideration (Chen et al., 2019; Krippendorff et al., 2009). Such coefficients were used to establish dependencies between biological activity and electronic properties.

Methods

Computational details

In this work, we downloaded X-ray structures of protein-ligand complexes from the Protein Data Bank (PDB codes: 1boz, 1hfp, 1kms, 3ghc, 3gi2, 3ntz, 3nu0, 4kfj, 4qhv, website – http://www.rcsb.org) (Cody et al., 1998, 2015; Gangjee et al., 1998, 2009; Klon et al., 2002; Lamb et al., 2013; Zhang et al., 2011) and extracted experimental IC_{50} values from The Binding Database. All IC_{50} values were converted to negative decimal logarithm (pIC_{50}) (Table 1). The optimization of the arrangement of hydrogen atoms is done by Chemosophia 'Hydrogens Positions Refinement' software (V. Potemkin & Grishina, 2018a; V. Potemkin et al., 2018) Chimera 1.13.1 (Pettersen et al., 2004) was used to compare the primary structures and for comparison and visualization of 3 D structures of the protein-ligand complexes.

The identification of intermolecular proteins-ligands interactions and the measurement of their bond length were carried out using a whole set of programs, such as: Chimera, Discovery Studio (Dassault Systèmes BIOVIA, 2015) and Protein-Ligand Interaction Profiler (PLIP) (Salentin et al., 2015). The confirmation of automated result obtained by this previously mentioned software was manually checked by Mercury (Macrae et al., 2008) software. The electronic characteristics were calculated using the AlteQ approach, which is described in detail in the next segment. The search for dependencies between these characteristics and the pIC_{50} was carried out using the Statistica (Statsoft.com, 2016) software.

AlteQ approach

The AlteQ approach (V. A. Potemkin & Grishina, 2008; V. Potemkin & Grishina, 2018a) represents the molecular electron density of the compound in space for a certain point m with coordinates x_m, y_m, z_m as a superposition of Slater-type electron density functions centered on each atom:

$$\rho(x_m, y_m, z_m) = \sum_{A=1}^{N} \rho_A \tag{1}$$

where N is the number of atoms in the molecular system, and ρ_A is the contribution of atom A to the electron density of the molecular system.

To determine the contribution of electron density for the elements of the Periodic system, three-dimensional electron density maps obtained for organic and inorganic compounds with atoms of the first, second, third and fifth periods using high-resolution low-temperature X-ray diffraction data were taken. Based on this, it was shown that the electron density contribution for elements can be represented by an equation:

$$\rho_A = \sum_{i=1}^{n_A} a_{Ai(s,p)} \exp\left(-b_{Ai(s,p)} R_A\right) + \sum_{i=3}^{n_A-1} a_{Ai(d)} \exp\left(-b_{Ai(d)} R_A\right) + \sum_{i=4}^{n_A-2} a_{Ai(f)} \exp\left(-b_{Ai(f)} R_A\right) \tag{2}$$

where the pairs $a_{Ai(s,p)}$ and $b_{Ai(s,p)}$, $a_{Ai(d)}$ and $b_{Ai(d)}$, $a_{Ai(f)}$ and $b_{Ai(f)}$ are the coefficients estimating the contributions of the s-, p-, d-, and f- orbitals of the A element in total electron density ρ_A; n_A is the principal number of the atom A, R_A is the distance between the center of the atom A and the point m, i is the number of shells of the s-, p-, d- and f-orbitals of A element, respectively.

Using the AlteQ approach (V. Potemkin et al., 2019), three-dimensional electron density maps were calculated to estimate various molecular and atomic characteristics using the Quantum Theory of Atoms in Molecules, or QTAIM, proposed by Bader (Bader, 1991; Kutzelnigg, 1992). This theory has already been successfully applied to the theoretical evaluation of molecular structures and the quantitative description of chemical bonds and their effects on reactivity and properties (Cukrowski et al., 2015; Saleh et al., 2015).

In this paper, we used the software 'Electron properties calculation: Integration over atomic basins' available on the site www.chemosophia.com using AlteQ electron density functions approach to obtain atomic characteristics. They are calculated based on radial integration over atomic basins. The integration starts from an atomic center and ends when the electron density surface reaches 0.001 a. u. or when the electron density is equal to the electron density of a neighboring atom. These characteristics include electrons of the j-th order overlaps in the atomic basin. The number of second-order overlap electrons in the atomic basin A is equal to:

Table 1. Showed the structure and pIC_{50} values of ligands-hDHFR.

Protein-ligand complex	Ligand	pIC_{50} (nM)
1boz	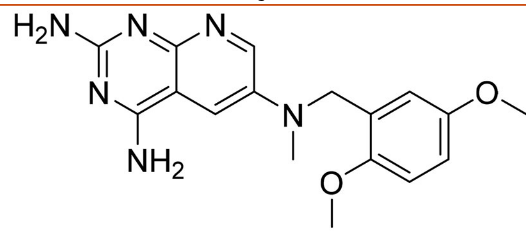	5.07
1hfp	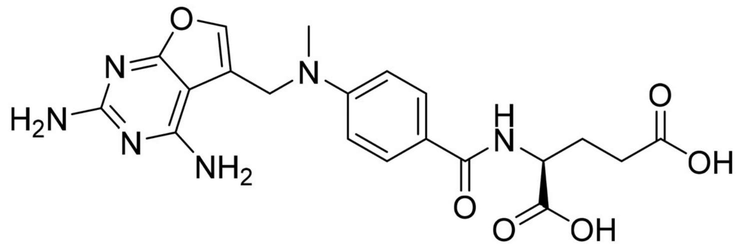	6.66
1kms	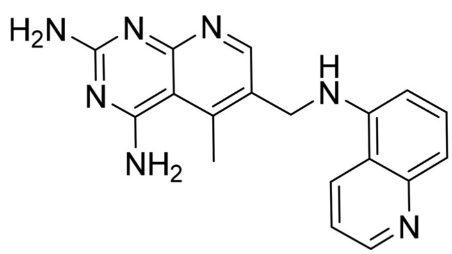	8.37
3ghc	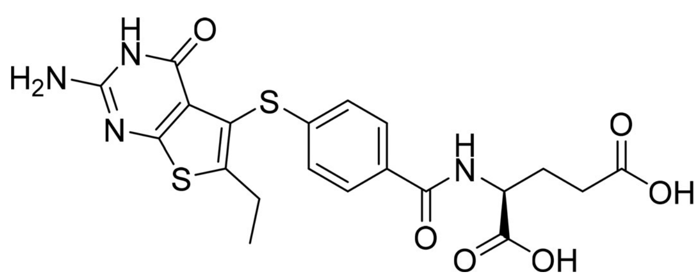	7.72
3gi2	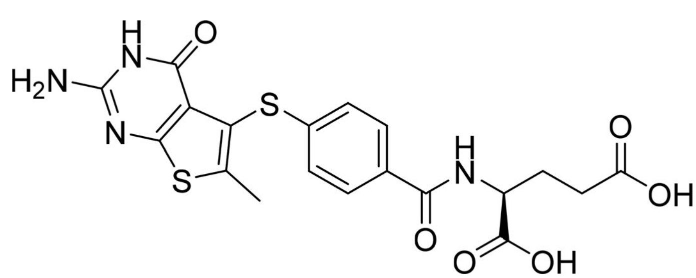	7.70
3ntz		7.05

(*continued*)

Table 1. Continued.

Protein-ligand complex	Ligand	pIC_{50} (nM)
	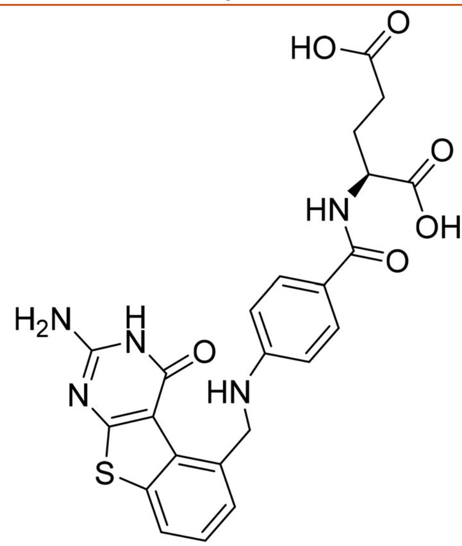	
3nu0	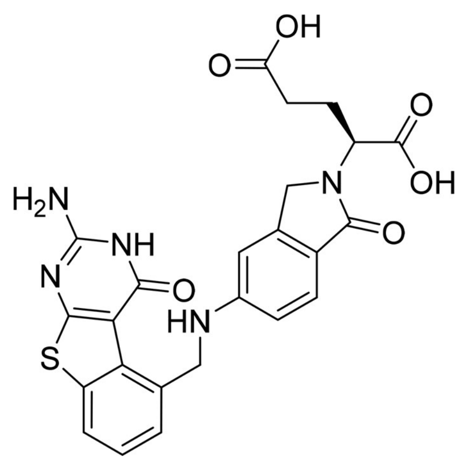	7
4kfj	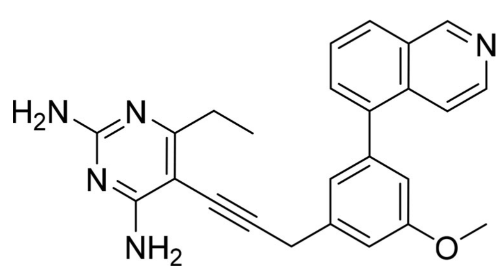	7.22
4qhv	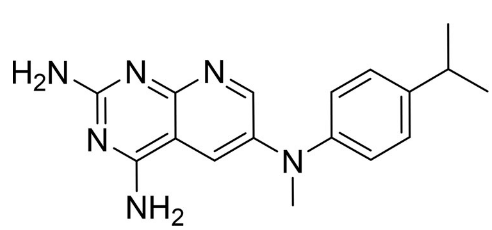	7.28

$$N_{A(1\cap 2)} = \int_{\Omega_A} \rho_{1\cap 2} dV \quad (3)$$

where dV is the instantaneous change in a volume, Ω_A is the atomic basin, and $\rho_{1\cap 2_m}$ is an electron density distribution function of the second order overlap of the first (A) and second (neighboring) atoms of the molecular system. It equals:

$$\rho_{1\cap 2} = min(\rho_1, \rho_2) \quad (4)$$

To calculate the number of electrons for the third, fourth, fifth, sixth and higher orders, similar equations are used. The isodensity surface area of *A* atom was found by the equation:

$$S_A(ext) = \int_{E_A} dS_A \quad (5)$$

where dS_A is an instantaneous change in the surface area, E_A is an isodensity surface with an electron density of 0.001 a.u.

The surface area of the separatrices was expressed by the following equation:

$$S_A(int) = \int_{I_A} dS \quad (6)$$

where I_A is the atomic separatrices.

Thus, the number of electrons belonging to the separatrices I_A, $N_A{}^S$ is defined as:

$$N_A^S = \int_{\boldsymbol{I_A}} \rho_A^S dS \quad (7)$$

where ρ_A^S is the electron density distribution function on the separatrice I_A.

Electrons of the second order overlap belonging to the separatrices I_A are computed as follows:

$$N_{A(1\cap 2)}^S = \int_{\boldsymbol{I_A}} \rho_{A(1\cap 2)}^S dS \quad (8)$$

where $\rho_{A(1\cap 2)}^S$ is an electron density distribution function of the second order overlap of the first (A) and second (neighboring) atoms on I_A atomic separatrice defined as

$$\rho_{A(1\cap 2)}^S = min(\rho_1^S,\ \rho_2^S) \quad (9)$$

The number of electron overlaps of the third, fourth, fifth, sixth and higher orders, which belong to the separatrices, are calculated in a similar way.

The number of own electrons of an atom *A* in its atomic basin equals:

$$N_A(own) = \int_{\Omega_A} \rho_A dV \quad (10)$$

The summary number of electrons of neighbors in the *A* atomic basin:

$$N_A(acc) = \int_{\Omega_A} \sum \rho_i dV \quad (11)$$

where ρ_i is the electron density distribution function of the *i*-th atom. The total number of electrons of the atom *A* in the basins of the neighbors can be found by the equation:

$$N_A(don) = \int_{\Omega_i} \rho_A dV \quad (12)$$

where Ω_i is the atomic basin of the *i*-th neighbor.

Thus, the total number of electrons of *A* atom in atomic overlaps:

$$N_A(overlaps) = N_A(acc) + N_A(don) \quad (13)$$

The total number of electrons in the *A* atomic basin:

$$N_A(total) = N_A(own) + N_A(acc) \quad (14)$$

Atomic charge – Q_A:

$$Q_A = N_A - N_A(total) \quad (15)$$

Volume of *A* atomic basin V_A equals:

$$V_A = \int_{\boldsymbol{\Omega_A}} dV \quad (16)$$

In addition, pair overlaps between *A* and *B* atoms can be calculated using the number of electrons of atom *A*, which are located in the basin of the adjacent atom $B(N_{B(B\cap A)})$, and the number of electrons of the neighboring atom B, which in turn are located in the basin of *A* atom $(N_{A(A\cap B)})$:

$$N_{B(B\cap A)} = \int_{\Omega_B} \rho_A dV \quad (17)$$

where Ω_B is the basin of the *B* atom.

$$N_{A(A\cap B)} = \int_{\Omega_A} \rho_B dV \quad (18)$$

For hDHFR complexes with ligands, the following molecular characteristics which are the sum of the above mentioned atomic characteristics were calculated: molecular volume (V_m), isodensity surface area (S_m), number of electrons of all considered atomic shells (N_e), number of own electrons in atomic basins (*Rom1*), number of electrons in atomic basins of the second, third, fourth, fifth and sixth orders overlaps (respectively, *Rom2*, *Rom3*, *Rom4*, *Rom5*, *Rom6*), positive and negative isodensity surface areas (S_{pm}, S_{nm}), the sum of the isodensity surface areas multiplied by the atomic charges for positively charged atoms (SQ_{pm}) and for negatively charged atoms (SQ_{nm}).

A set of electronic descriptors allowing to estimate the increment of each atomic type observed in organic compounds (i.e. H, C, N, O, P, S, F, Cl, Br, I) in molecular electronic properties was suggested. For example V_α – sums of volumes of atoms of α type, S_α – isodensity surface area of atoms of α type, Ro_α – the number of electrons in atomic basin of atoms of α type, $Ro1_\alpha$ – number of own electrons in α atomic basins, $Ro2_\alpha$, $Ro3_\alpha$, $Ro4_\alpha$ atoms, $Ro5_\alpha$ and $Ro6_\alpha$ are the numbers of electrons of atomic basins of α type atoms participating in the overlaps of the second, third, fourth, fifth and sixth orders respectively, $Ronei_\alpha$ is the number of electrons of neighboring atoms in the atomic basins of α type, $Roon_\alpha$ is the number of electrons of atoms of α type in the basins of neighbors, positive and negative isodensity surface areas of atoms of α type ($S_{p\alpha}$, $S_{n\alpha}$), the sum of the isodensity surface areas multiplied by the atomic charges for positively charged atoms of α type ($SQ_{p\alpha}$) and for negatively charged atoms of α type ($SQ_{n\alpha}$).

Also, using the AlteQ approach, electronic characteristics were calculated separately for complexes, for ligands and for complexes without ligands to calculate changes in each electronic descriptor during complex formation (dS_m, dV_m, dN_e, *dRom1*, *dRom2*, *dRom3*, *dRom4*, *dRom5*, *dRom6*, dS_{pm}, dS_{nm}, dSQ_{pm}, dSQ_{nm}, dV_α, dS_α, dRo_α, $dRo1_\alpha$, $dRo2_\alpha$, $dRo3_\alpha$, $dRo4_\alpha$, $dRo5_\alpha$, $dRo6_\alpha$, $dRonei_\alpha$, $dRoon_\alpha$), by the following general equation:

$$dD_m = D - D_m(lig) - D_m(enz) \quad (19)$$

where *D* is total descriptor of interest, $D_m(lig)$ and $D_m(enz)$ are the same descriptors, calculated only for the ligand and the complex without the ligand, respectively.

Hydrogens positions refinement

The method was created for the search of the optimal localization of hydrogens in molecular systems. It is based on QM/MM approach suggested by Nobel Prize winners – A. Warshel, M. Karplus and M. Levitt (Warshel & Karplus, 1972; Warshel & Levitt, 1976). For QM/MM computations, we used MM3 molecular mechanics force field (Ponder & Richards, 1987) and modification of AlteQ quantum chemical method, namely AlteQ-G method (V. Potemkin & Grishina, 2018a), for estimation of Gibbs free energy. AlteQ-G Gibbs free energies are computed from electron overlaps $N_{A\cap B}$, $N_{A\cap B\cap C}$, etc. evaluated using approximation of AlteQ Slater type electron density functions #2 with Gaussians – φ_A φ_B, etc:

$$\rho_A \approx \varphi_A = \sum_{i=l}^{k} a'_{Ai} * \exp\left(-b'_{Ai} * R_A^2\right) \tag{20}$$

where a'_{Ai} *and* b'_{Ai} are AlteQ-G parameters (V. Potemkin & Grishina, 2018a).

$$N_{el\ A}^{Sur} = \frac{\partial N_{el\ A}^{in}}{\partial R_A} = \frac{\partial N_A}{\partial R_A} - \sum_{A<B} \frac{\partial N_{A\cap B}}{\partial R_A} + \sum_{A<B<C} \frac{\partial N_{A\cap B\cap C}}{\partial R_A} - \sum_{A<B<C<D} \frac{\partial N_{A\cap B\cap C\cap D}}{\partial R_A} + \dots \tag{21}$$

where

$$N_{A\cap B\dots} = 4\pi \int_0^\infty \varphi_A \varphi_B \dots R^2 dR \tag{22}$$

Different publications demonstrate the sufficient quality of assessment of enthalpy, entropy, Gibbs free energy, liquid density, pKa values of bases and acids of organic and inorganic compounds, photovoltaic properties of dye-sensitized solar cells, bond orders, ionization potentials, molar ionization energies by AlteQ and AlteQ-G approaches (M. A. Grishina & Potemkin, 2019; M. Grishina et al., 2016; V. Potemkin & Grishina, 2018a; V. Potemkin et al., 2019; V. Potemkin et al., 2019; E. Salmina et al., 2013; E. S. Salmina et al., 2011; Slepukhin et al., 2013). Recently, it has been shown that the methods demonstrate good reproducibility of 3 D maps of electron density of organic and inorganic compounds derived from low temperature high resolution X-ray diffraction data. The quality of the assessment of 3 D electron density maps by the AlteQ method is not inferior and even exceeds the quality of the assessment by widely used methods of quantum chemistry of high levels of theory, for example DFT B3LYP/6-311G(d,p) and HF/6-311G(d,p) for organic compounds, 3-21 G for compounds containing heavy elements, e.g. (V. A. Potemkin & Grishina, 2008; V. Potemkin & Grishina, 2018a). Furthermore, the method was successfully applied to study properties of large biomolecular systems (M. A. Grishina & Potemkin, 2019; Pathak et al., 2020), properties and surface morphology of nanoparticles of inorganic compounds and their complexes with organic dyes (M. Grishina et al., 2016; V. Potemkin et al., 2019), QSAR and QSPR problems (A. V. Potemkin et al., 2017; V. Potemkin & Grishina, 2018b; V. Potemkin et al., 2019), enzyme-ligand complementarity (Rimac et al., 2020).

Molecular dynamics (MD) simulations

The 3-D coordinates of co-crystallized hDHFR and ligands complexes were analyzed using the MD simulations based algorithms implemented in GROMACS 2018-2 molecular mechanics package (Van Der Spoel et al., 2005). The GROMOS96 53a6 force field was used for the parameterization of hDHFR protein structures (Oostenbrink et al., 2004). Additionally, the topologies of co-crystallized ligands were generated using PRODRG server (Schüttelkopf & van Aalten, 2004), with the correction of the partial charges was performed using the DFT method present in GAUSSIAN software suite with B3LYP 6-31 G (d,p) basis set in combination with CHELPG program (Frisch et al., 2009). The periodic conditions were generated and the system was solvated using the SPC/E water model (Zielkiewicz, 2005) present in GROMACS. The successive step involves the neutralization which involve the addition of suitable number of NA and CL counter ions. Consequently, the energy minimization step was performed using combined steepest descent and conjugate gradient algorithms, with a convergence criterion of 0.005 kcal/mol, and the position restraints were applied to the structure of INH. Thereafter, the system was equilibrated in combination with NVT (constant volume) and NPT (constant pressure) ensemble conditions, each at 100 ps time scale. The temperature of 300 K was maintained for the system using Berendsen weak coupling method, and the pressure of 1 bar was maintained utilizing Parrinello-Rahman barostat in the equilibration stage. The LINCS algorithm was used for the generation of the final conformational production stage for 50 ns timescale, and trajectories were generated, which were analyzed in order to understand the behavior of each complex in the explicit water environment. The behavior of various hDHFR-ligand complexes was observed in the form of calculated parameters such as H-bonds, Root Mean Square Deviation (RMSD), and Radius of Gyration (Rg). Furthermore, the Molecular mechanics Poisson–Boltzmann surface area (MM-PBSA) protocols implemented in g_mmpbsa package (Kumari et al., 2014) were used for the calculation of total free energy of binding between hDHFR and co-crystallized ligands.

Results and discussion

Relation of pIC50 values to AlteQ characteristics

A large set of electronic properties was calculated using AlteQ approach. Then experimental pIC_{50} values were related to the properties. Thus, for this purpose, we particularly choose one-factor quantitative models, which describes pIC_{50} values with high correlation coefficients.

Change in total volume (dV_m) was found by Equation (19). The relationship between pIC_{50} and dV_m is well established and described through linear regression model (Figure 1) with correlation coefficient −0.78:

$$pIC_{50} = 4.1448 - 0.0583 * dV_m \tag{23}$$

Further, the results revealed that pIC_{50} value increases with the dV_m value decrease and vice-versa. The results also confirmed that small deviations in the position of amino acid

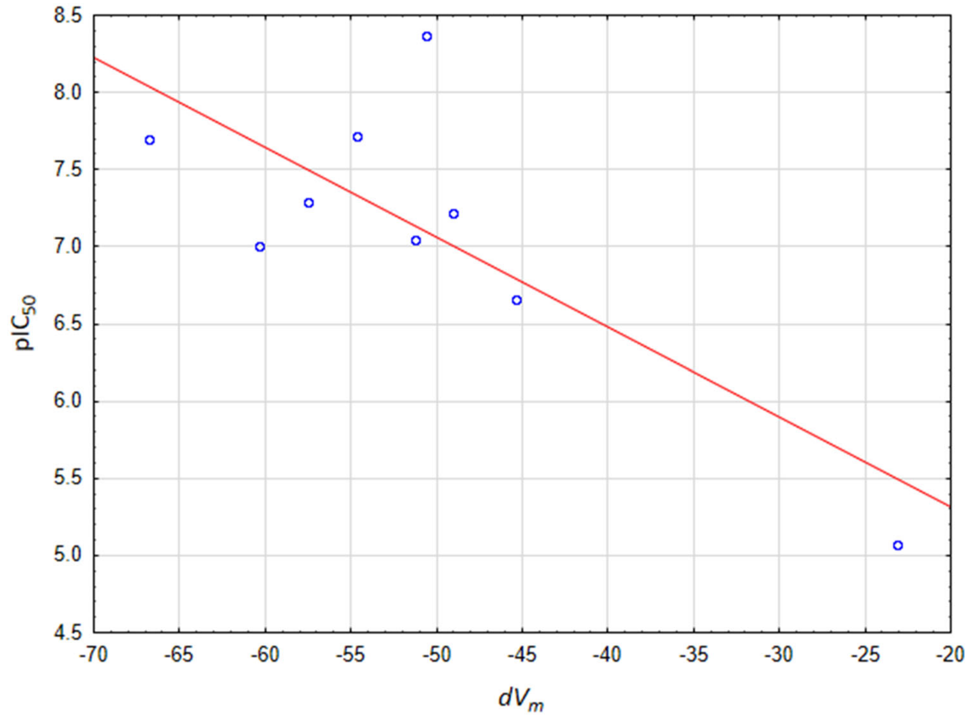

Figure 1. The relationship between the change in total volume (dV_m) and the negative decimal logarithm of half maximal inhibitory concentration (pIC_{50}).

have considerable impact on bioactivity. This propensity can be explained by the fact that the bond formation between ligands and proteins decreases the overall volume of the complexes. In simplest term, it means that the more effective binding enforces smaller changes in volume $–dV_m$, and consequently increases pIC_{50}.

Furthermore, the next descriptor – $dRo1_H$ (the change in the number of own electrons of hydrogen atoms in their atomic basins of complexes as compared to the unbound enzyme and the ligand) also showed good correlation with the bioactivity (pIC_{50})value such as dV_m. The change in $Ro1_H$ was obtained by Equation (19). The relationship between pIC_{50} and $dRo1_H$ was also expressed through linear regression model with considerable correlation coefficient (–0.73):

$$pIC_{50} = 1.7800 - 6.0556 * dRo1_H \tag{24}$$

The graphical illustration of the relationship is displayed in Figure 2. The analysis also showed the similar pattern as dV_m and illustrated inverse relationship between $dRo1_H$ and pIC_{50}.

We are conscious about the fact that insertion of any carefully designed ligand into the protein pocket promotes the formation of intermolecular bonds and results the overlapping of atomic electron shells. This shows that the number of electrons not involved in the bond formation decreases in complexes as compared to the unbound ligand and enzyme. The result showed that the smaller number of electrons not participating in bond formation promotes potential efficiency for binding and resulting lower $dRo1_H$ and higher pIC_{50}.

The tendencies of dependency of pIC_{50} with $dV_m$and $dRo1_H$ look logical. On one hand, the formation of favorable interactions (covalent, hydrogen-bonded, van der Waals, Coulomb, etc.) is characterized by a decrease in the length of contacts and increase of electron overlaps. This determines a simultaneous decrease in the volume and in the number of inner electrons not involved in overlapping of basins of contacting atoms. Hydrogen atoms are located on the periphery of the molecule. Therefore, they primarily determine the interactions between the ligand and enzyme. Figure 3 shows a good linear relationship between the factors dV_m and $dRo1_H$ ($R^2 = -0.73$).

On the other hand, when a complex has effective interactions, its total volume and number of electrons not participating in the overlaps of basins are smaller than the analogues descriptors for unbound ligands and the enzymes. Therefore, more effective interactions with the largest reduction in V_m and $Ro1_H$ have correspondingly the minimum values of $dV_m$and $dRo1_H$ and are typically the most active molecules with a higher pIC_{50} values. Importance of hydrogen atoms' contribution to the overlap of the enzyme and ligand is reflected by high correlation coefficient between $dRo1_H$ and pIC_{50}.

Nevertheless, for more acurate prediction of activity the entire spectrum of interactions in the enzyme-ligand system involving non-hydrogen atoms has to be incorporated into the model. For this reason, pair overlaps of atomic orbitals of all intermolecular bonds between ligands and proteins of these complexes were calculated to determine more effective contacts.

The additional analysis allowed us to determine two parts of the enzyme (Figure 4), which when interacting with ligand leads to a decrease of pIC_{50}. The decision to group these residues into two groups is based upon their position relative to the ligands.

It was found that the number of all electrons involved in the overlap between the ligand and both parts A and B

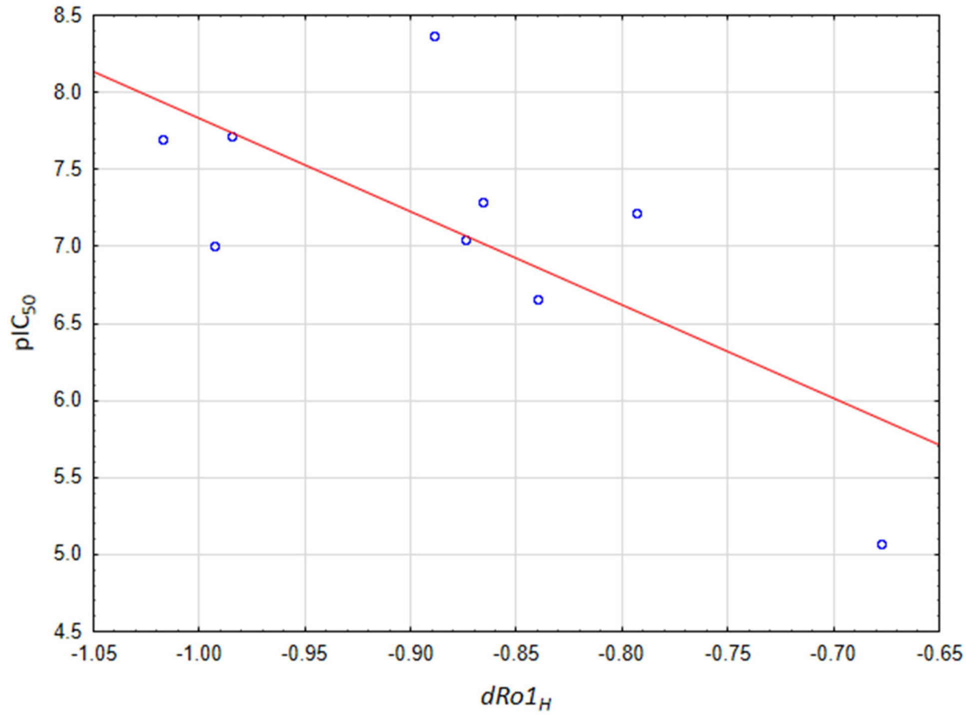

Figure 2. The dependency of the number of own electrons of hydrogen atoms in their own atomic basins ($dRo1_H$) and the negative decimal logarithm of half maximal inhibitory concentration (pIC_{50}).

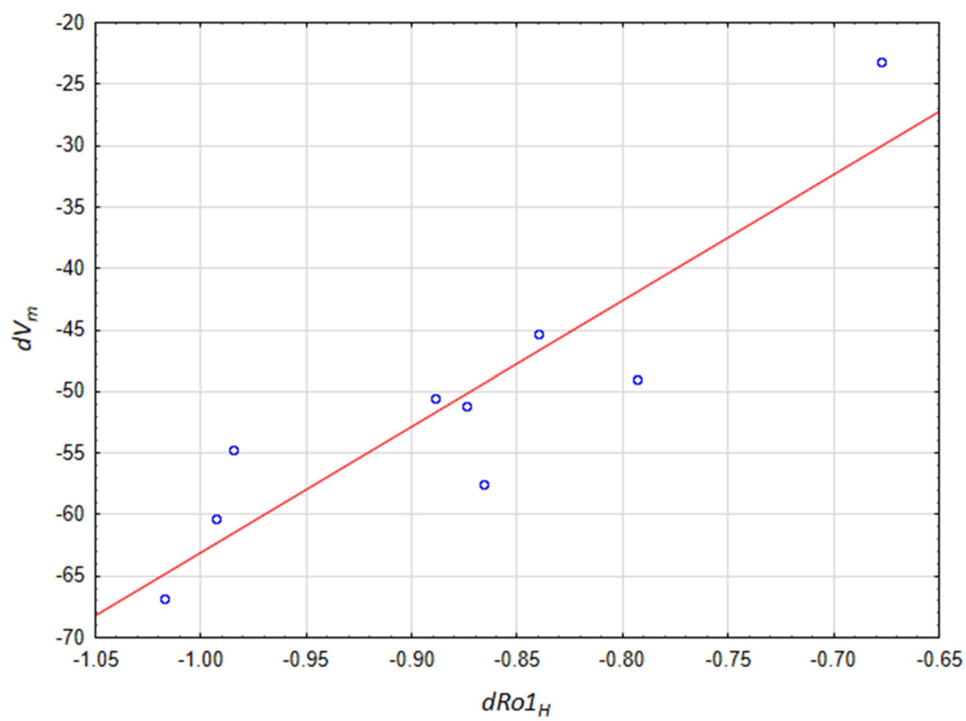

Figure 3. The relationship between the number of own electrons of hydrogen atoms in their own atomic basins ($dRo1_H$) and the change in total volume (dV_m).

($N_{SideA+B}(lig)$) correlates highly with pIC_{50}. The data values areplottedagainst each other on Figure 5. The corresponding linear regression model has correlation coefficient of0.91:

$$pIC_{50} = 12.72 - 14.71 * N_{SideA+B}(lig) \tag{25}$$

The careful inspection of intermolecular interactions, pointed out that the **1boz**, **1hfp** proteins are different from the **1kms-4qhv** proteins.Namely, the **1boz** and **1hfp** proteins, with the lowest pIC_{50} values,has Gly31 instead of Phe31. Upon further investigation of the protein tertiary structure, an interaction was found between one of the two ligands rings of the **1kms-4qhv** complexes and the Phe31 phenyl ring. This kind of interactions has already been noted by previous studies(Cao et al., 2018; Klon et al., 2002). Figure 5 shows that those two points with the lowest bioactivity (**1boz**, **1hfp**) have greater overlap. This reflects the

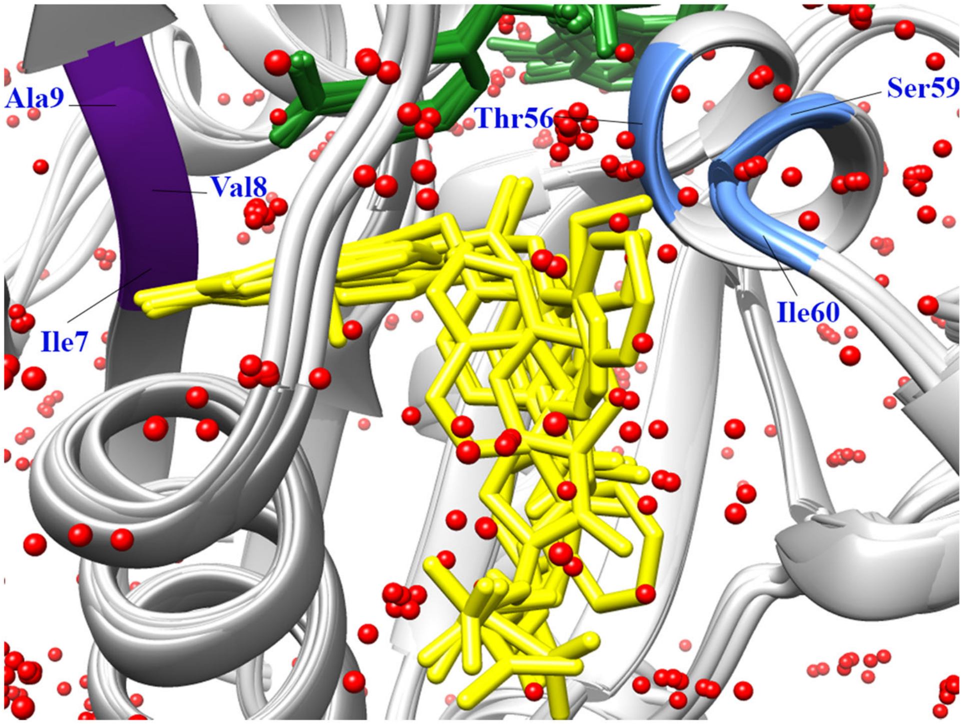

Figure 4. Active side of merged **1boz-4qhv**; light blue – part A (Thr56, Ser59 and Ile60); purple – part B (Ile7, Val8 and Ala9) gray – the rest of residues; yellow – ligands; red – water; green – NADPH.

fact that their ligands do not form intermolecular bonds with Phe31 because of its absence and the ligand monocyclic fragments form stronger interactions with part B residues, due to the fact that Gly31 does not contain a cyclic system that could complicate the binding.

Furthermore, Figure 5 illustrates that two points (**4kfj**, **4qhv**) deviate from the obtained line. The point **4kfj** binds weaker to the residues of parts A and B, however, it has a lower bioactivity than some of the other complexes. It motivated us to look for alternative reasons decreasing bioactivity. First reason is associated with the steric factor, namely, the bulky substituents of the pyrimidine ring including the methoxyphenylene and isoquinoline rings, which prevents deeper penetration of the ligand into the receptor cavity and better binding.Secondly, the isoquinoline ring forms CH$\cdots\pi$ bonds with Leu67, which are not observed among other considered complexes, which may affect the pIC_{50} value as well.

For **4qhv** it was found that the ligand N-methyl group forms strong CH$\cdots\pi$ intermolecular interactions with NADPH, as evidenced by the overlap ($N_{NADPH}(lig)$) of the ligand and cofactor. $N_{NADPH}(lig)=$ 0.32 for **4qhv**, and the values lying in the range of $0.11-0.21$ a.u. for the rest of the dataset. The strong interaction with NADPH can compensate for influence of overlaps between ligand and parts A, B, and increase pIC_{50}.

Further in-depth studies highlight the residue Ile60, as the one that influences the most the pIC_{50}value, compared to the other residues in parts A and B. A dependency relating pIC_{50} and the number of all electrons involved in the overlap between the ligand and Ile60 ($N_{Ile60}(lig)$) has been found, with a correlation coefficient of -0.84 (Figure 6):

$$pIC_{50} = 8.8199 - 20.594 * N_{Ile60}(lig) \quad (26)$$

The data shows that decline in overlaps of a ligand and Ile60 amino acid residue leads to greater pIC_{50}. Moreover, the $N_{Ile60}(lig)$ values of **1boz** and **1hfp** are the lowest among the studied complexes (Figure 6). Ile60 residue is located oppositely to the Phe31 residue, proving that the phenyl ring of Phe31 influencethe binding between a ligand and Ile60.

By inspection and comparison of crystal structures, we noticed the presence of water molecules in a vicinity of ligand, so we explored the possibility that water molecules could influence on pIC_{50}. The suggestion was proved by the dependence (Figure 7). This is characterized by the Langmuir isotherm I type equation, the correlation coefficient of which is 0.93 (Figure 7):

$$pIC_{50} = -49.684 + \frac{2.9429 * N_{Wat}(lig)}{5.052 * 10^{-2} * N_{Wat}(lig) + 4.4259 * 10^{-4}} \quad (27)$$

It follows that the greater overlaps of the water molecules and a ligand lead to the higher pIC_{50}.

Most studies, for example (Lamb et al., 2013; Raimondi et al., 2019; Volpato et al., 2009), suggest that the binding to Phe31 directly leads to greater pIC_{50}. Since, Phe31 is lipophilic it prefers hydrophobic ligands. Furthermore, the strength of overlapbetween ligand and Phe31 does not influence on pIC_{50}. For instance, the number of all electrons involved in the overlaps between the ligand and Phe31 of the complexes with the highest bioactivity ($N_{Phe31}(lig)_{1kms}$, $N_{Phe31}(lig)_{3ghc}$) and one of the complexes with the lowest bioactivity ($N_{Phe31}(lig)_{3ntz}$) are approximately the same and lie in

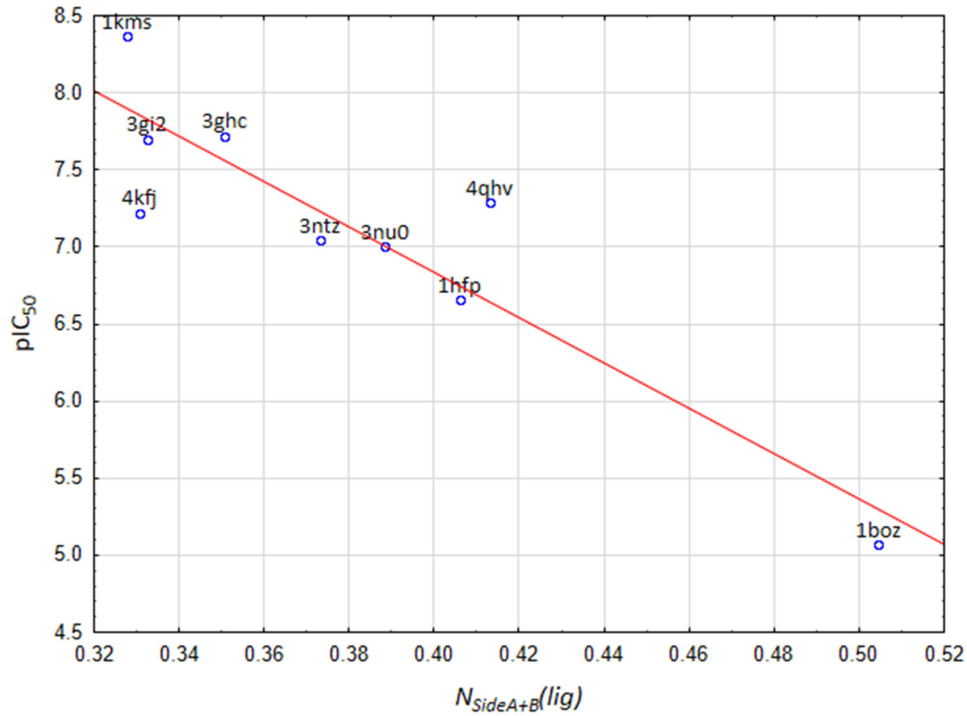

Figure 5. The dependency of all electrons involved in the overlap between the ligand and both parts A and B ($N_{SideA+B}(lig)$) and the negative decimal logarithm of half maximal inhibitory concentration (pIC_{50}).

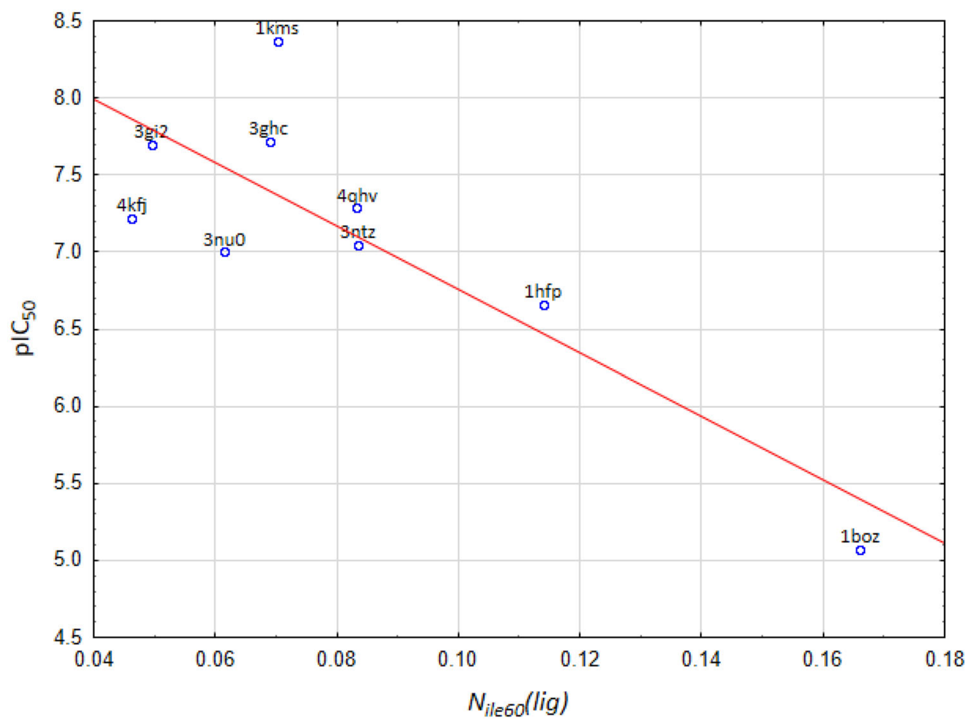

Figure 6. The dependency of all electrons involved in the overlap between the ligand and both Ile60 ($N_{Ile60}(lig)$) and the negative decimal logarithm of half maximal inhibitory concentration (pIC_{50}).

0.13 – 0.14 a.u. range, while the rest of the values is in the range between 0.15 – 0.35 a.u. and do not establish any dependence.On the other hand, the complexes with Gly31 (**1boz**, **1hfp**) have the lowest pIC_{50}. During the study, we identified the region (Position **1** on Figure 8(b)), where water molecules form hydrogen bonds with Glu30, Trp27 and a ligand (Figure 8).This location is present in all complexes except for **1boz** and **1hfp**. In the case of **1boz** there is a water molecule next to the position **1**, however, it only binds to N5 atom and do not form hydrogen bonds with Glu30 and Trp27. As for **1hfp**, no water molecules are present in position **1** (Figure 8(a)).

The studies done by Rodd and Cummins teams (Cummins & Gready, 2001; Rod & Brooks, 2003) show that the water molecules of hDHFR-Folate complex from position **1** participate in N5 atom protonation ofFH2 by Glu30 as in the case

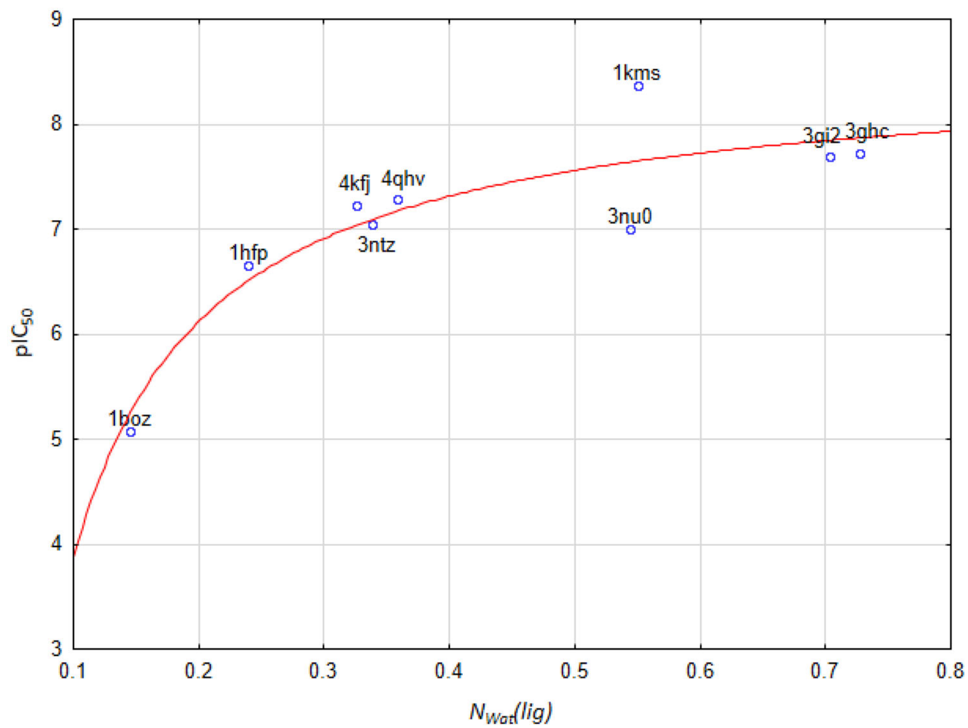

Figure 7. The relationship between pIC_{50} and the number of all electrons involved in the overlaps between the ligand and all water molecules ($N_{Wat}(lig)$).

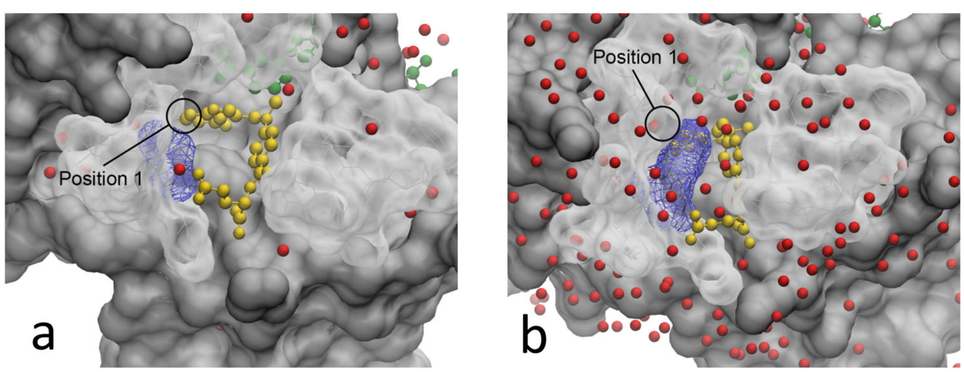

Figure 8. (a) Active side of **1hfp**; blue – Gly31; gray – the rest of residues; yellow – ligand; red – water; green – NADPH, (b) Active side of **3ghc**; blue – Phe31; gray – the rest of residues; yellow – ligand; red – water; green – NADPH.

of Asp27 in *E. coli* DHFR pattern. Our assumption is that Phe31 influence on pIC_{50} indirectly in two ways (Figure 8(b)). The first one is that when the ligand enters the binding pocket it displaces water molecule inside and bulky phenyl ring of Phe31 blocks the leaving of the water molecule from **1**. Thus, the complexes with Gly31 do not have water molecules in **1**, because there is not any huge substituent to impede the leaving of water molecules and keep it inside for the protonation stage. The second kind of influence is that interactions between Phe31 and water molecules in **1** decrease the maneuverability of these water molecules. Since they are partially confined, they can bind to Glu30, Trp27 and a ligand.Water molecules can only weakly bind to Gly31 and Gly31 cannot keep them in position **1** during a sufficient time for binding to parts of receptor (Glu30) and ligand (heteroatoms of the main ring), which participate in water mediated hydrogen transfer (Cummins & Gready, 2001; Rod & Brooks, 2003).

Another region (Position **2** on Figure 9(a)) was found with conserved water molecule, where water is linked with a ligand and NADPH. Water molecule inthis area is observed in all complexes except for **1boz** and **4qhv** (Figure 9). The atomic overlaps between ligands, NADPH and water molecules in position**2** ($N_{Wat2+NADPH}(lig)$) were compared to the pIC_{50}, and were found they correlate well with each other ($R^2 = 0.88$, Figure 10):

$$pIC_{50} = 4.6123 + 8.3276 * N_{Wat2+NADPH}(lig) \quad (28)$$

The established model shows that the larger the overlapping between ligand, NADPH and water molecule in position **2** is the greater is the bioactivity.

In complex with the highest bioactivity (**1kms**), it was noticed that the ligand atom N10 forms strong hydrogen bond with water molecule in position**2**, and has the greatest overlap with it ($N_{Wat2}(lig)_{1kms}$= 0.11 a.u.). The water molecule from position**2** in **3ghc-3nu0**complexes also makes strong intermolecular hydrogen bonds with S8 (**3ghc, 3gi2**) and N11 (**3ntz, 3nu0**).

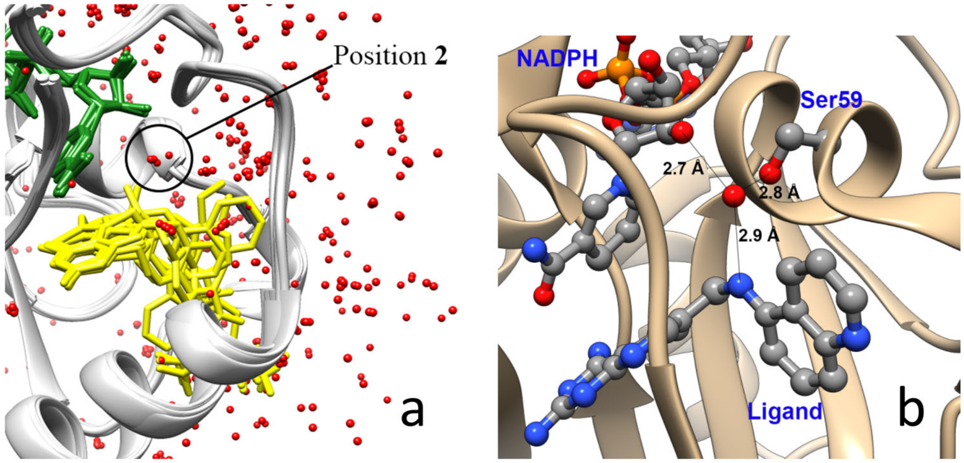

Figure 9. (a) Active side of merged **1boz-4qhv**; gray – the rest of residues; yellow – ligands; red – water; green – NADPH, (b) Distances between the closest interacted atoms of water molecule in position **2**, ligand, NADPH and enzyme in **1kms**; angles: ∠LigWatNADPH = 144.91°, ∠LigWatSer59 = 102.77°, ∠Ser59WatNADPH = 97.63°.

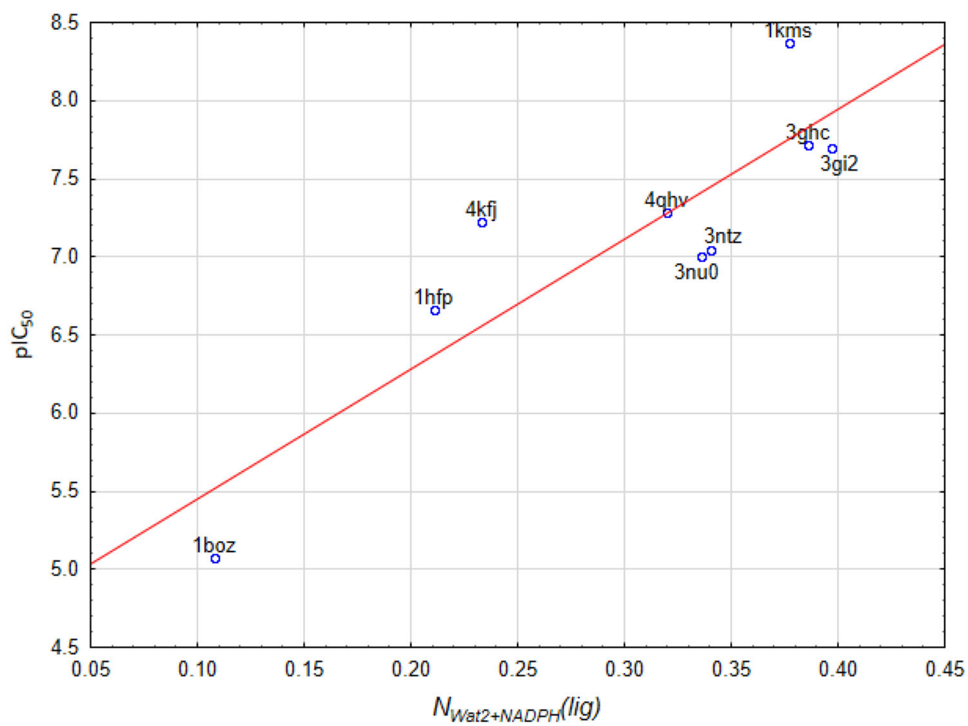

Figure 10. The number of all electrons involved in the overlap between the ligand, NADPH and water molecule in **2** ($N_{Wat2+NADPH}(lig)$) and pIC_{50}.

Those overlaps are of similar scale (in the range of 0.08 – 0.09 a.u.), but lower than corresponding $N_{Wat2}(lig)_{1kms}$.

The methoxyphenylene ring of ligand in complex **4kfj** can bind to position **2** water with only by $\pi\cdots$H-O interaction, that much weaker than hydrogen bond ($N_{Wat2}(lig)_{4kfj} = 0.05$ a.u.). Other complexes cannot form any intermolecular connections (**1hfp**) or do not have the water molecule in position**2** (**1boz**, **4qhv**) because of the N-methyl groups instead of N-hydrogen atoms, which are observed in **1kms**, **3ntz** and **3nu0**. In view of the above, it means that the interaction with water in position **2** play a crucial role in inhibition of hDHFR and strongly affects pIC_{50}.

Indeed, the ligand of **1kms** has the largest overlap with water molecule from region **2**. At the same time, the overlap between the ligand and NADPH is 0.17 a.u., what is bit lower then analogous overlap in **3ghc** and **3gi2**, which equal to 0.20 a.u. and 0.21 a.u., respectively.

Furthermore, as the highest value of overlap belongs to **4kfj**, it follows that the geometry of N-methyl group may contribute to a formation of bonds and increase the bioactivity. Thus, $N_{NADPH}(lig)$ can be viewed as a secondary factor influencing on pIC_{50}, and it is better to address this descriptor with $N_{Wat2}(lig)$ in total ($N_{Wat2+NADPH}(lig)$).

Structural dynamics and QM/MM modeling of hDHFR and ligand complexes

The MD simulations techniques were explored for a better understanding of the structural basis of inhibition between

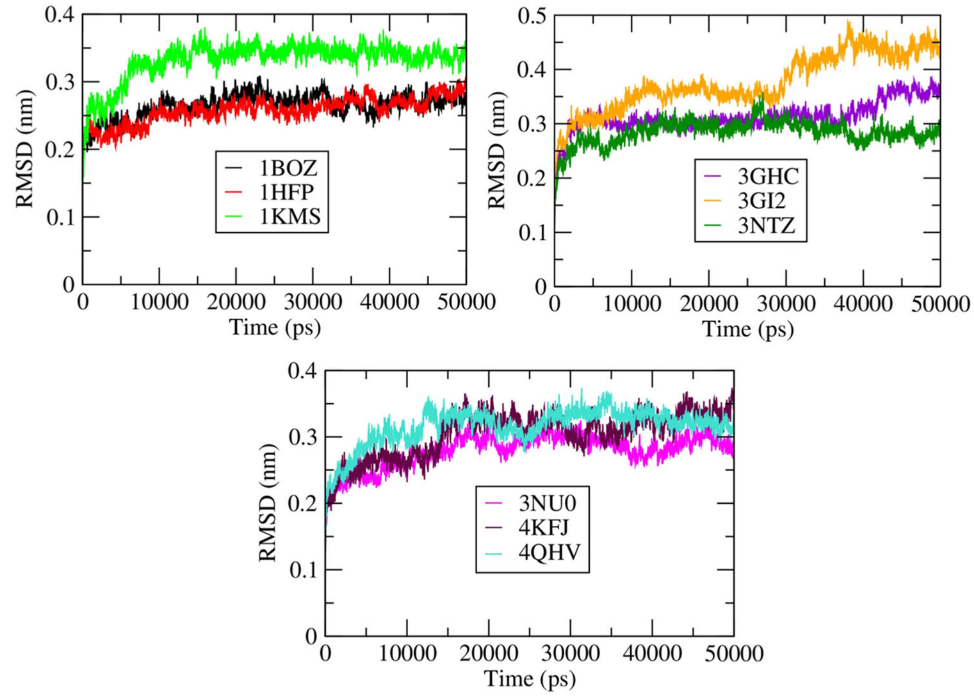

Figure 11. The graphs illustrating the changes in the RMSD values generated after 50 ns MD simulation analyses.

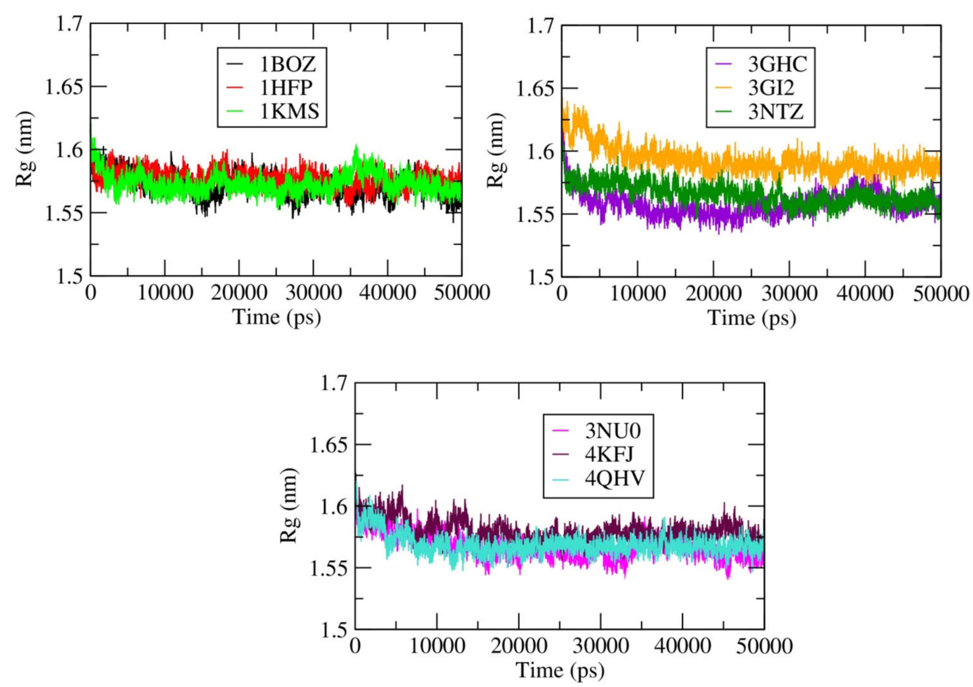

Figure 12. The Rg value curves highlighting the changes in the compactness of the studied hDHFR and co-crystallized ligand systems.

Table 2. List of MD simulation-based generated parameters highlighting the relative affinities observed between the hDHFR and co-crystallized ligands.

S. no.	Protein-ligand complex (PDB IDs	Hydrogen bonds	Total free energy (kJ/mol)	**Short contact between N of the ligand and H of the hDHFR (Å)**
	1boz	14	−510.17	2.02
	1hfp	16	−460.27	1.91
	1kms	16	−452.73	1.87
	3ghc	14	−461.34	1.79 with water
	3gi2	4	−282.71	1.89
	3ntz	15	−466.83	1.90
	3nu0	14	−467.09	1.90
	4kfj	16	−462.20	2.17
	4qhv	17	−511.76	1.87

hDHFR and co-crystallized ligands to a higher extent, which involved the immersion of crystallized complex systems in the explicit water solvent conditions, and the conformational dynamics of all nine systems were studied for 50 ns time scale (Total 450 ns). Primarily, the structural stability of all the systems was evaluated in terms of changes in the RMSD values, which showed that 1kms and **3gi2** systems were observed to be more unstable as compared to the rest (Figure 11), as higher fluctuation in the RMSD values were observed for the respective systems.

Similarly, the Rg values were calculated which is a measure to evaluate the structural compactness of hDHFR and co-crystallized ligands systems during MD simulations. The Rg was calculated as the mass-weighted root mean square of the atomic distance from their collective center of mass (Sneha & George Priya Doss, 2016). The degrees of compactness achieved in the studied complexed hDHFR proteins were highlighted in Figure 12. All the systems showed a relatively similar level of compactness which is indicative of the fluctuating Rg values between 1.55 nm − 1.6 nm. The 3ghc, in particular, achieved the highest compactness as the Rg values were observed below 1.55 nm showed the attainment of the highest stability of the system.

Furthermore, the affinities of hDHFR with the adjoined ligands were analyzed in terms of the calculated hydrogen bonds and total free energy of binding (Table 2). Relatively similar binding affinities were observed for all the studied systems except 3gi2 in which the calculated hydrogen bonds were observed to be around 4 and the total free energy of interaction was −282.71 kJ/mol. The 4qhv system showed comparatively higher binding affinity which is indicative from the calculated hydrogen bonds of around 17 and free energy of −511.76 kJ/mol. These observations the binding of ligands with hDHFR is highly energy favorable.

The structures of the complexes and their characteristics obtained using MD simulations and obtained using QM/MM approach, namely 'Hydrogens Position Refinement' were compared to each other. We found that both types of computations indicated a short contact between nitrogen of heterocyclic system of ligands and hydrogen of carboxyl group of the GLU30 of the enzyme. The distance varies between 1.89 and 2.17 Å (Table 2). The interactions may indicate a protonated state of the ligand at the moment of interaction with the receptor. An exception is the complex 3ghc in which there is a short contact between O of CO-group of the ligand and the hydrogen atom of water, which in its tern forms hydrogen bond with the enzyme and acts as a proton carrier. The results of modeling are in a good agreement with the results of investigations of other authors, e.g. (Cocco et al., 1983; Ghaleb et al., 2020; Shah et al., 2019; Threadgill et al., 1987). Model complexes are presented in Supplementary materials.

Conclusions

We reviewed the AlteQ computational methodology, designed to fast and accurately calculation of electron characteristics for macromolecular systems. This approach was adopted for 9 complexes of human DHFR protein with ligands bound into the active site, whose structures were obtained from the PDB database. The correlations between calculated descriptors and experimentally determined pIC_{50} values were successfully established. For electron descriptors showing changes in the complex volume and changes in the number of electrons of ligand hydrogen atoms in their own atomic basins, the correlation coefficients of −0.78 and −0.73, respectively, were obtained. The phenyl ring of Phe31 affects pIC_{50} indirectly, and not directly by binding to the inhibitor, as was previously thought. A bulky side chain substituent blocks the exit of water molecules required for protonation in position **1** and reduces their mobility due to O-H$\cdots\pi$ contacts. Despite the hydrophobicity of the active site of the protein, interaction of water molecules with a ligand, plays a critical role in inhibiting hDHFR, especially for waters from positions **1** and **2**. In addition to water contacts, the formation of favorable intermolecular interactions between the inhibitor and NADPH cofactor can lead to an increase in the activity.

Acknowledgment

The authors are very thankful for Taif University researcher supporting project Number TURSP/91, Taif University, Taif, Saudi Arabia.

Disclosure statement

The authors have declared that there is no conflict of interest.

Funding

The project was supported by Act 211 Government of the Russian Federation, contract 02.A03.21.0011, and Ministry of Science and Higher Education of the Russian Federation (Grant no – FENU-2020-0019).

ORCID

Vladislav Naumovich http://orcid.org/0000-0001-5446-3527
Maria Grishina http://orcid.org/0000-0002-2573-4831
Jurica Novak http://orcid.org/0000-0001-5744-6677
Prateek Pathak http://orcid.org/0000-0002-6160-9755
Vladimir Potemkin http://orcid.org/0000-0002-5244-8718
Mohd Shahbaaz http://orcid.org/0000-0001-8901-7113
Magda H. Abdellattif http://orcid.org/0000-0002-8562-4749

References

Abdelaziz, O. A., El Husseiny, W. M., Selim, K. B., & Eisa, H. M. (2019). Dihydrofolate reductase inhibition effect of 5-substituted pyrido[2,3-d]pyrimidines: Synthesis, antitumor activity and molecular modeling study. *Bioorganic Chemistry*, *90*, 10307 6. https://doi.org/10.1016/j.bioorg.2019.103076

Arooj, M., Sakkiah, S., Cao, G., Ping., & Lee, K. W. (2013). An innovative strategy for dual inhibitor design and its application in dual inhibition of human thymidylate synthase and dihydrofolate reductase enzymes. *PLoS One*, *8*(4), e60470. https://doi.org/10.1371/journal.pone.0060470

Bader, R. F. W. (1991). A quantum theory of molecular structure and its applications. *Chemical Reviews*, *91*(5), 893–928. https://doi.org/10.1021/cr00005a013

Cao, H., Gao, M., Zhou, H., & Skolnick, J. (2018). The crystal structure of a tetrahydrofolate-bound dihydrofolate reductase reveals the origin of slow product release. *Communications Biology*, *1*(1), 226. https://doi.org/10.1038/s42003-018-0236-y

Cario, H., Smith, D. E. C., Blom, H., Blau, N., Bode, H., Holzmann, K., Pannicke, U., Hopfner, K.-P., Rump, E.-M., Ayric, Z., Kohne, E., Debatin, K.-M., Smulders, Y., & Schwarz, K. (2011). Dihydrofolate reductase deficiency due to a homozygous DHFR mutation causes megaloblastic anemia and cerebral folate deficiency leading to severe neurologic disease. *American Journal of Human Genetics*, *88*(2), 226–231. https://doi.org/10.1016/j.ajhg.2011.01.007

Chen, X., Liu, M., Wen, S., Lin, Y., Nicola, G. (2019). *Binding database*. http://www.bindingdb.org

Cocco, L., Roth, B., Temple, C., Montgomery, J. A., London, R. E., & Blakley, R. L. (1983). Protonated state of methotrexate, trimethoprim, and pyrimethamine bound to dihydrofolate reductase. *Archives of Biochemistry and Biophysics*, *226*(2), 567–577. https://doi.org/10.1016/0003-9861(83)90326-0

Cody, V., Galitsky, N., Luft, J. R., Pangborn, W., Blakley, R. L., & Gangjee, A. (1998). Comparison of ternary crystal complexes of F31 variants of human dihydrofolate reductase with NADPH and a classical antitumor furopyrimidine. *Anti-Cancer Drug Design*, *13*(4), 307–315.

Cody, V., Pace, J., Namjoshi, O. A., & Gangjee, A. (2015). Structure-activity correlations for three pyrido[2,3-d]pyrimidine antifolates binding to human and Pneumocystis carinii dihydrofolate reductase. *Acta Crystallographica. Section F, Structural Biology Communications*, *71*(Pt 6), 799–803. https://doi.org/10.1107/S2053230X15008468

Cukrowski, I., de Lange, J. H., Adeyinka, A. S., & Mangondo, P. (2015). Evaluating common QTAIM and NCI interpretations of the electron density concentration through IQA interaction energies and 1D cross-sections of the electron and deformation density distributions. *Computational and Theoretical Chemistry*, *1053*, 60–76. https://doi.org/10.1016/j.comptc.2014.10.005

Cummins, P. L., & Gready, J. E. (2001). Energetically most likely substrate and active-site protonation sites and pathways in the catalytic mechanism of dihydrofolate reductase. *Journal of the American Chemical Society*, *123*(15), 3418–3428. https://doi.org/10.1021/ja0038474

Dassault Systèmes BIOVIA. (2015). *Discovery studio visualizer*. Dassault Systèmes.

Etienne, M.-C., Ilc, K., Formento, J.-L., Laurent-Puig, P., Formento, P., Cheradame, S., Fischel, J.-L., & Milano, G. (2004). Thymidylate synthase and methylenetetrahydrofolate reductase gene polymorphisms: Relationships with 5-fluorouracil sensitivity. *British Journal of Cancer*, *90*(2), 526–534. https://doi.org/10.1038/sj.bjc.6601523

Frisch, M. J., Trucks, G. W., Schlegel, H. B., Susceria, G. E., Robb, M. A., Cheeseman, J. R., Scalmani, G., Barone, V., Petersson, G. A., Nakatsuji, H., Caricato, M., Li, X., Hratchian, H. P., Izmaylov, A. F., Bloino, J., Zheng, G., Sonnenberg, J. L., Williams-Young, D. … Fox, C. (2009). *Gaussian 09*. Gaussian, Inc.

Gangjee, A., Li, W., Kisliuk, R. L., Cody, V., Pace, J., Piraino, J., & Makin, J. (2009). Design, synthesis, and X-ray crystal structure of classical and nonclassical 2-amino-4-oxo-5-substituted-6-ethylthieno[2,3-d]pyrimidines as dual thymidylate synthase and dihydrofolate reductase inhibitors and as potential antitumor agents. *Journal of Medicinal Chemistry*, *52*(15), 4892–4902. https://doi.org/10.1021/jm900490a

Gangjee, A., Qiu, Y., Li, W., & Kisliuk, R. L. (2008). Potent dual thymidylate synthase and dihydrofolate reductase inhibitors: Classical and nonclassical 2-amino-4-oxo-5-arylthio-substituted-6-methylthieno[2,3-d]pyrimidine antifolates. *Journal of Medicinal Chemistry*, *51*(18), 5789–5797. https://doi.org/10.1021/jm8006933

Gangjee, A., Vidwans, A. P., Vasudevan, A., Queener, S. F., Kisliuk, R. L., Cody, V., Li, R., Galitsky, N., Luft, J. R., & Pangborn, W. (1998). Structure-based design and synthesis of lipophilic 2,4-diamino-6-substituted quinazolines and their evaluation as inhibitors of dihydrofolate reductases and potential antitumor agents 1. *Journal of Medicinal Chemistry*, *41*(18), 3426–3434. https://doi.org/10.1021/jm980081y

Ghaleb, A., Aouidate, A., Ayouchia, H. B. E., Aarjane, M., Anane, H., & Stiriba, S.-E. (2020). In silico molecular investigations of pyridine N-Oxide compounds as potential inhibitors of SARS-CoV-2: 3D QSAR, molecular docking modeling, and ADMET screening. *Journal of Biomolecular Structure and Dynamics*, 1–11. https://doi.org/10.1080/07391102.2020.1808530

Grishina, M., Bolshakov, O., Potemkin, A., & Potemkin, V. (2016). Theoretical investigation of electron structure and surface morphology of titanium dioxide anatase nano-particles. *Computational and Theoretical Chemistry*, *1091*, 122–136. https://doi.org/10.1016/j.comptc.2016.07.003

Grishina, M. A., & Potemkin, V. A. (2019). Topological analysis of electron density in large biomolecular systems. *Current Drug Discovery Technologies*, *16*(4), 437–448. https://doi.org/10.2174/1570163815666180821165330

Hashkes, P. J., Becker, M. L., Cabral, D. A., Laxer, R. M., Paller, A. S., Rabinovich, C. E., Turner, D., & Zulian, F. (2014). Methotrexate: New uses for an old drug. *The Journal of Pediatrics*, *164*(2), 231–236. https://doi.org/10.1016/j.jpeds.2013.10.029

Hawser, S., Lociuro, S., & Islam, K. (2006). Dihydrofolate reductase inhibitors as antibacterial agents. *Biochemical Pharmacology*, *71*(7), 941–948. https://doi.org/10.1016/j.bcp.2005.10.052

Huber, M., & Huber, B. (2019). Innovation in oncology drug development. *Journal of Oncology*, *2019*, 9683016. https://doi.org/10.1155/2019/9683016

Klon, A. E., Héroux, A., Ross, L. J., Pathak, V., Johnson, C. A., Piper, J. R., & Borhani, D. W. (2002). Atomic structures of human dihydrofolate reductase complexed with NADPH and two lipophilic antifolates at 1.09Å and 1.05Å resolution. *Journal of Molecular Biology*, *320*(3), 677–693. https://doi.org/10.1016/S0022-2836(02)00469-2

Krippendorff, B. F., Neuhaus, R., Lienau, P., Reichel, A., & Huisinga, W. (2009). Mechanism-based inhibition: Deriving K(I) and k(inact) directly from time-dependent IC(50) values. *Journal of Biomolecular Screening*, *14*(8), 913–923. https://doi.org/10.1177/1087057109336751

Kumari, R., Kumar, R., & Lynn, A. (2014). g_mmpbsa-a GROMACS tool for high-throughput MM-PBSA calculations. *Journal of Chemical Information and Modeling*, *54*(7), 1951–1962. https://doi.org/10.1021/ci500020m

Kutzelnigg, W. (1992). Atoms in molecules. A quantum theory. (Reihe: International Series of Monographs on Chemistry, Vol. 22.) Von R.F.W. Bader. Clarendon Press, Oxford, 1990. XVIII, 438 S., geb. £50.00. – ISBN 0-19-855168-1. *Angewandte Chemie*, *104*(10), 1423–1423. https://doi.org/10.1002/ange.19921041040

Lamb, K. M., G-Dayanandan, N., Wright, D. L., & Anderson, A. C. (2013). Elucidating features that drive the design of selective antifolates using crystal structures of human dihydrofolate reductase. *Biochemistry*, *52*(41), 7318–7326. https://doi.org/10.1021/bi400852h

Longley, D. B., Latif, T., Boyer, J., Allen, W. L., Maxwell, P. J., & Johnston, P. G. (2003). The interaction of thymidylate synthase expression with p53-regulated signaling pathways in tumor cells. *Seminars in Oncology*, *30*(3 Suppl 6), 3–9. https://doi.org/10.1016/s0093-7754(03)00119-2

Macrae, C. F., Bruno, I. J., Chisholm, J. A., Edgington, P. R., McCabe, P., Pidcock, E., Rodriguez-Monge, L., Taylor, R., van de Streek, J., & Wood, P. A. (2008). Mercury CSD 2.0 – New features for the visualization and investigation of crystal structures. *Journal of Applied Crystallography*, *41*(2), 466–470. https://doi.org/10.1107/S0021889807067908

Masters, P. A., O'Bryan, T. A., Zurlo, J., Miller, D. Q., & Joshi, N. (2003). Trimethoprim-sulfamethoxazole revisited. *Archives of Internal Medicine*, *163*(4), 402–410. https://doi.org/10.1001/archinte.163.4.402

Nduati, E., Diriye, A., Ommeh, S., Mwai, L., Kiara, S., Masseno, V., Kokwaro, G., & Nzila, A. (2008). Effect of folate derivatives on the activity of antifolate drugs used against malaria and cancer. *Parasitology Research*, *102*(6), 1227–1234. https://doi.org/10.1007/s00436-008-0897-4

Oostenbrink, C., Villa, A., Mark, A. E., & Van Gunsteren, W. F. (2004). A biomolecular force field based on the free enthalpy of hydration and solvation: The GROMOS force-field parameter sets 53A5 and 53A6. *Journal of Computational Chemistry*, *25*(13), 1656–1676. https://doi.org/10.1002/jcc.20090

Padma, V. V. (2015). An overview of targeted cancer therapy. *BioMedicine*, *5*(4), 19. https://doi.org/10.7603/s40681-015-0019-4

Pathak, P., Naumovich, V., Grishina, M., & Potemkin, V. (2020). The study of EGFR-ligand complex electron property relationship with biological activity. *Journal of Biomolecular Structure and Dynamics*, 1–14. https://doi.org/10.1080/07391102.2020.1813629

Pettersen, E. F., Goddard, T. D., Huang, C. C., Couch, G. S., Greenblatt, D. M., Meng, E. C., & Ferrin, T. E. (2004). UCSF Chimera-a visualization system for exploratory research and analysis. *Journal of Computational Chemistry*, *25*(13), 1605–1612. https://doi.org/10.1002/jcc.20084

Ponder, J. W., & Richards, F. M. (1987). An efficient newton-like method for molecular mechanics energy minimization of large molecules. *Journal of Computational Chemistry*, *8*(7), 1016–1024. https://doi.org/10.1002/jcc.540080710

Potemkin, V., & Grishina, M. (2018a). Electron-based descriptors in the study of physicochemical properties of compounds. *Computational and Theoretical Chemistry*, *1123*, 1–10. https://doi.org/10.1016/j.comptc.2017.11.010

Potemkin, V., & Grishina, M. (2018b). Grid-based technologies for in silico screening and drug design. *Current Medicinal Chemistry*, *25*(29), 3526–3537. https://doi.org/10.2174/0929867325666180309112454

Potemkin, V., Palko, N., & Grishina, M. (2019). Quantum theory of atoms in molecules for photovoltaics. *Solar Energy*, *190*, 475–487. https://doi.org/10.1016/j.solener.2019.08.048

Potemkin, V. A., & Grishina, M. A. (2008). A new paradigm for pattern recognition of drugs. *Journal of Computer-Aided Molecular Design*, *22*(6–7), 489–505. https://doi.org/10.1007/s10822-008-9203-x

Potemkin, V. A., Grishina, M. A., & Potemkin, V. A. (2017). Grid-based continual analysis of molecular interior for drug discovery, QSAR and QSPR. *Current Drug Discovery Technologies*, *14*(3), 181–205. https://doi.org/10.2174/1570163814666170207144018

Potemkin, V. A., Pogrebnoy, A. A., & Grishina, M. A. (2009). Technique for energy decomposition in the study of “receptor-ligand” complexes. *Journal of Chemical Information and Modeling*, *49*(6), 1389–1406. https://doi.org/10.1021/ci800405n

Potemkin, V., Potemkin, A., & Grishina, M. (2018). Internet resources for drug discovery and design. *Current Topics in Medicinal Chemistry*, *18*(22), 1955–1975. https://doi.org/10.2174/1568026619666181129142127

Raimondi, M., Randazzo, O., La Franca, M., Barone, G., Vignoni, E., Rossi, D., & Collina, S. (2019). DHFR inhibitors: Reading the past for discovering novel anticancer agents. *Molecules*, *24*(6), 1140. https://doi.org/10.3390/molecules24061140

Rimac, H., Grishina, M. A., & Potemkin, V. A. (2020). Electron density analysis of CDK complexes using the AlteQ method. *Future Medicinal Chemistry*, *12*(15), 1387–1397. https://doi.org/10.4155/fmc-2020-0076

Rod, T. H., & Brooks, C. L. (2003). How dihydrofolate reductase facilitates protonation of dihydrofolate. *Journal of the American Chemical Society*, *125*(29), 8718–8719. https://doi.org/10.1021/ja035272r

Saleh, G., Gatti, C., & Lo Presti, L. (2015). Energetics of non-covalent interactions from electron and energy density distributions. *Computational and Theoretical Chemistry*, *1053*, 53–59. https://doi.org/10.1016/j.comptc.2014.10.011

Salentin, S., Schreiber, S., Haupt, V. J., Adasme, M. F., & Schroeder, M. (2015). PLIP: Fully automated protein-ligand interaction profiler. *Nucleic Acids Research*, *43*(W1), W443–W447. https://doi.org/10.1093/nar/gkv315

Salmina, E., Grishina, M. A., & Potemkin, V. A. (2013). An approximation of the Cioslowski–Mixon bond order indexes using the AlteQ approach . *Journal of Computer-Aided Molecular Design*, *27*(9), 793–805. https://doi.org/10.1007/s10822-013-9677-z

Salmina, E. S., Rusinov, G. L., Slepukhin, P. A., Ishmetova, R. I., Tolshchina, S. G., Potemkin, V. A., & Grishina, M. A. (2011). Intermolecular interactions in heteromolecular crystals of tetrazine derivatives with azoles. *Journal of Structural Chemistry*, *52*(6), 1134–1138. https://doi.org/10.1134/S0022476611060187

Schober, A. F., Mathis, A. D., Ingle, C., Park, J. O., Chen, L., Rabinowitz, J. D., Junier, I., Rivoire, O., & Reynolds, K. A. (2019). A two-enzyme adaptive unit within bacterial folate metabolism. *Cell Reports*, *27*(11), 3359–3370.e7. https://doi.org/10.1016/j.celrep.2019.05.030

Schüttelkopf, A. W., & van Aalten, D. M. F. (2004). PRODRG: A tool for high-throughput crystallography of protein-ligand complexes. *Acta Crystallographica. Section D, Biological Crystallography*, *60*(Pt 8), 1355–1363. https://doi.org/10.1107/S0907444904011679

Shah, K., Queener, S., Cody, V., Pace, J., & Gangjee, A. (2019). Development of substituted pyrido[3,2-d]pyrimidines as potent and selective dihydrofolate reductase inhibitors for pneumocystis pneumonia infection. *Bioorganic & Medicinal Chemistry Letters*, *29*(15), 1874–1880. https://doi.org/10.1016/j.bmcl.2019.06.004

Singh, A., Deshpande, N., Pramanik, N., Jhunjhunwala, S., Rangarajan, A., & Atreya, H. S. (2018). Optimized peptide based inhibitors targeting the dihydrofolate reductase pathway in cancer. *Scientific Reports*, *8*(1), 3190. https://doi.org/10.1038/s41598-018-21435-5

Slepukhin, P. A., Salmina, E. S., Potemkin, V. A., & Grishina, M. A. (2013). Crystal and electronic structure of heteromolecular complexes of 3,6-bis(3,5-dymethylpyrazole-1-yl)-1,2,4,5-tetrazine with azoles. *Journal of Structural Chemistry*, *54*(6), 1091–1100. https://doi.org/10.1134/S0022476613060139

Sneha, P., & George Priya Doss, C. (2016). Molecular Dynamics: New Frontier in Personalized Medicine. *Advances in Protein Chemistry and Structural Biology*, *102*, 181–224. https://doi.org/10.1016/bs.apcsb.2015.09.004

Statsoft.com. (2016). *STATISTICA*. TIBKO Software inc.

Stivarou, T., Grazia Cipolleschi, M., D'Amico, M., Mannini, A., Mini, E., Rovida, E., Dello Sbarba, P., Olivotto, M., & Marzi, I. (2015). The complex metabolic network gearing the G1/S transition in leukemic stem cells: Hints to a rational use of antineoplastic agents. *Oncotarget*, *6*(31), 31985–31996. https://doi.org/10.18632/oncotarget.5155

Threadgill, M. D., Griffin, R. J., Stevens, M. F. G., & Wong, S. K. (1987). Structural studies on bio-active compounds. Part 6. Determination of the sites of protonation on three 2,4-diaminopyrimidines of pharmaceutical importance by proton-coupled 13C and 1H nuclear magnetic resonance spectroscopy. *Journal of the Chemical Society, Perkin Transactions*, 1, 2229. https://doi.org/10.1039/p19870002229

Van Der Spoel, D., Lindahl, E., Hess, B., Groenhof, G., Mark, A. E., & Berendsen, H. J. C. (2005). GROMACS: Fast, flexible, and free. *Journal of Computational Chemistry*, *26*(16), 1701–1718. https://doi.org/10.1002/jcc.20291

Volpato, J. P., Yachnin, B. J., Blanchet, J., Guerrero, V., Poulin, L., Fossati, E., Berghuis, A. M., & Pelletier, J. N. (2009). Multiple conformers in active site of human dihydrofolate reductase F31R/Q35E double mutant suggest structural basis for methotrexate resistance. *The Journal of Biological Chemistry*, *284*(30), 20079–20089. https://doi.org/10.1074/jbc.M109.018010

Warshel, A., & Karplus, M. (1972). Calculation of ground and excited state potential surfaces of conjugated molecules. I. Formulation and parametrization. *Journal of the American Chemical Society*, *94*(16), 5612–5625. https://doi.org/10.1021/ja00771a014

Warshel, A., & Levitt, M. (1976). Theoretical studies of enzymic reactions: Dielectric, electrostatic and steric stabilization of the carbonium ion in the reaction of lysozyme. *Journal of Molecular Biology*, *103*(2), 227–249. https://doi.org/10.1016/0022-2836(76)90311-9

Zhang, X., Zhou, X., Kisliuk, R. L., Piraino, J., Cody, V., & Gangjee, A. (2011). Design, synthesis, biological evaluation and X-ray crystal structure of novel classical 6,5,6-tricyclic benzo[4,5]thieno[2,3-d]pyrimidines as dual thymidylate synthase and dihydrofolate reductase inhibitors. *Bioorganic & Medicinal Chemistry*, *19*(11), 3585–3594. https://doi.org/10.1016/j.bmc.2011.03.067

Zielkiewicz, J. (2005). Structural properties of water: Comparison of the SPC, SPCE, TIP4P, and TIP5P models of water. *The Journal of Chemical Physics*, *123*(10), 104501. https://doi.org/10.1063/1.2018637